# Influence of inlet contraction ratios on the heat transfer and pressure drop characteristics of single-phase flow in smooth circular tubes in the transitional flow regime

AI Bashir, M Everts and JP Meyer[*]

Department of Mechanical and Aeronautical Engineering, University of Pretoria, Pretoria, 0002, South Africa.

[*]Author for correspondence, e-mail: josua.meyer@up.ac.za

## Highlights

• Effect of flow-calming section contents on the transitional flow regime.

• Comparison between square-edged, re-entrant, fully developed and 90° bend inlets.

• Inlet contraction ratios affects the boundaries of the transitional flow regime.

## Abstract

An experimental investigation of the single-phase heat transfer and pressure drop characteristics in the transitional flow regime has been performed using flow-calming sections with different inlet geometries and section-to-tube inlet contraction ratios. Four different types of inlets were investigated namely a square-edged, re-entrant, a hydrodynamically fully developed inlet, and a 90º bend inlet. The contraction ratios for the squared-edged and re-entrant inlets were 5, 11, 15 and 33. For the hydrodynamically fully developed inlet and the 90º bend inlet, a contraction ratio of one was used. Experiments were conducted using a circular test section with an inner diameter of 5.1 mm, at a Reynolds number range of 1 000 to 6 000 to ensure that the laminar, transitional, quasi-turbulent and turbulent flow regimes were covered. Water was used as the working fluid and the test section was heated at constant wall heat fluxes of 4, 6 and 8 kW/m$^2$. It was found that for a square-edged inlet geometry, the transition from the laminar to the turbulent flow regimes occurred earlier as the inlet contraction ratio increased, while for the re-entrant inlet, transition was delayed. The transitional flow regime was significantly affected by smaller contraction ratios and this effect increased with increasing heat flux. However, it was found that the critical Reynolds numbers were independent of inlet geometry for contraction ratios larger than 33. For the 90º bend inlet, transition occurred earlier than all the other inlet geometries and contraction ratios.

**Keywords:** Square-edged inlet, Re-entrant inlet, Flow-calming section, Contraction ratio, Pressure drop, Heat transfer, Transitional flow regime, Elbow.

## Nomenclature

| | |
|---|---|
| $b$ | Bulk |
| $C_p$ | Specific heat at constant pressure |
| $D$ | Diameter |
| $eb$ | Energy balance error |
| $f$ | Friction factor |
| FD | Fully Developed |
| $g$ | Gravitational acceleration |
| $Gr$ | Grashof number |
| $Gr^*$ | Modified Grashof number |
| $h$ | Heat transfer coefficient |
| $I$ | Current |
| $i$ | Data point index |
| $j$ | Colburn $j$-factor |
| $k$ | Thermal conductivity |
| $L$ | Length |
| $\dot{m}$ | Mass flow rate |
| $Nu$ | Nusselt number |
| $P$ | Pressure |
| $Pr$ | Prandtl number |
| $P_w$ | Modified tube wall parameter |
| $\dot{Q}$ | Heat transfer rate |
| $\dot{q}$ | Heat flux |
| $R$ | Thermal resistance |
| $Ra$ | Rayleigh Number |
| $Re$ | Reynolds number |
| $T$ | Temperature |
| $t$ | Tube thickness |
| $V$ | Voltage |
| $x$ | Distance from tube inlet |

**Special characters**

| | |
|---|---|
| $\beta$ | Coefficient of thermal expansion |
| $\mu$ | Dynamic viscosity |
| $\rho$ | Density |

**Subscripts**

| | |
|---|---|
| $avg$ | Average |
| $b$ | Bulk |
| $Cu$ | Copper |
| $cr$ | Critical |
| $e$ | Exit |
| $f$ | Fluid/friction factor |
| FD | Fully developed |
| $i$ | Inlet/inner/data point index |
| $iw$ | Inner wall |
| $Nu$ | Nusselt number |
| $o$ | Outer |
| $ow$ | Outer wall |
| $\Delta P$ | Pressure drop |
| $qt$ | Quasi-turbulent |
| $ree$ | Re-entrant |
| $squ$ | Square-edged |
| $t$ | Thermal |
| $w$ | Wall |

## 1. Introduction

Heat exchangers are widely used in industries such as power generation, HVAC systems, manufacturing plants, transport systems (automotive, trains, aeroplanes and ships), oil, gas and chemical processing. Most heat exchangers operate in the turbulent flow regime and occasionally in the laminar or even transitional flow regimes. Although the transitional flow regime is associated with high uncertainties, it is sometimes unavoidable in heat exchangers due to design constraints, system upgrades, fouling or even changes in operating conditions that lead to lower mass flow rates.

The transitional flow regime has been receiving great attention in recent years due to its good compromise between high heat transfer and low pressure drop [1], making it a potential heat exchanger operating flow regime. Several articles [2-14] have been published in recent years on the characteristic behaviour of heat transfer and pressure drop in the transitional flow regime under various operating conditions. The influence of heating, buoyancy, inclination and inlet geometry on the transition from laminar to turbulent flow regimes were extensively investigated. The Reynolds number boundaries of the transitional flow regime were quantified, and heat transfer coefficient and friction factor correlations have been developed for both forced and mixed convection heat transfer. However, because it was found that the heat transfer and pressure drop characteristics in the transitional flow regime were significantly affected by the inlet geometry, different correlations were developed for different inlet geometries.

Ghajar and his co-workers were the pioneers of the work on the effect of inlet disturbances on the heat transfer and pressure drop characteristics in the transitional flow regime of smooth horizontal tubes. Three different inlet configurations were investigated namely: square-edged, re-entrant and bell-mouth. To ensure a uniform upstream flow to the different inlet geometries, a flow-calming section was attached prior to the inlet section. A constant flow-calming section diameter was used throughout the experiments with a contraction ratio of approximately 10.

For the re-entrant inlet geometry, the test section was slid one diameter into the inlet section, as found typically in the headers of shell and tube heat exchangers. For the square-edged inlet, which is found in most heat exchangers, there was a sudden contraction at the inlet section to the test section. To avoid the formation of eddies at the inlet of the test section, the bell-mouth inlet consisted of a smooth and gradual contraction from the flow-calming section diameter to the test section diameter. Some of these works can be found in [2, 4-6, 13, 15-19] and summarized in the

3

text book of Cengel and Ghajar [20]. The experiments were conducted at different constant heat fluxes. In general, the heat transfer and pressure drop characteristics, as well as the boundaries of the transitional flow regime, were significantly affected by the inlet geometries. However, the influence of different inlet contraction ratios on each inlet geometry was not investigated. Changing the contraction ratio could change the magnitude of upstream flow disturbances in the flow-calming and inlet sections.

Meyer and his co-workers were the second group of researchers that worked on the characteristic behaviour of heat transfer and pressure drop in the transitional flow regime of smooth and enhanced tubes, focussing on inlet geometry effects [9, 10, 21, 22], buoyancy effects [7, 11, 23], inclination angles [23], enhancement with twisted tape inserts [9, 24, 25] and annular flow [26]. These analyses involved both cooling and heating conditions under constant wall temperature and constant heat flux boundary conditions, mostly with flow-calming sections and different inlet contraction ratios. Meyer et al. [9] conducted experiments with multiple circular tubes under constant heat flux conditions. The purpose was to investigate the influence of flow maldistribution at the inlet of multiple tubes, as well as tube protrusion in relation to the adjacent tubes, on the heat transfer and pressure drop characteristics in the laminar, transitional and turbulent flow regimes. It was found that as the pitch ratio increased, the critical Reynolds numbers and transition gradients of the side tubes decreased due to decrease in flow asymmetry. For a square-edged inlet, transition in the centre tube was delayed compared to a single tube. Furthermore, a protrusion of the centre tube increased the asymmetry of the flow in the side tubes and therefore increased their critical Reynolds numbers and transition gradients. The experiments were conducted using a flow-calming section with a large contraction ratio of approximately 58, to avoid any effects of the inlet header geometry. It can be expected that the use of different or lower inlet contraction ratios, typically found in many practical settings, might again influence the flow asymmetry and affect the behaviour and boundaries of the transitional flow regime.

Dirker et al. [10] investigated the effect of inlet geometries on the boundaries of the transitional flow regime, as well as the heat transfer and pressure drop characteristics, in micro-channels heated at a constant heat flux. Three inlet contraction ratios (5, 6.25 and 10) were investigated with a bell-mouth inlet only and one contraction ratio each for sudden contraction and swirl inlets. It was found that for the bell-mouth inlet, transition was delayed as the contraction ratio decreased from 10 to 5. In general, all the inlet geometries significantly affected the heat transfer and pressure drop characteristics in the laminar and transitional flow regimes.

Other researchers also investigated the influence of inlet geometries and disturbances not only on the transitional flow regime but also on the laminar and turbulent flow regimes. Nagendra [27] studied the influence of inlet turbulence on the mixed convection heat transfer in the transitional and turbulent flow regimes of a smooth horizontal tube. The inlet disturbances were introduced by placing an inlet probe near the inlet. It was found that the inlet disturbances caused transition to occur earlier but had no influence in the turbulent flow regime. However, for $ReRa(D_i/L)$ larger than $10^6$, it was found that the inlet disturbances had no influence on any of the flow regimes. Mori et al. [28] also found that the level of the inlet turbulence significantly affected the critical Reynolds numbers and it changed with Rayleigh number. For large $ReRa$, the inlet disturbances had no influence.

Al-arabi [29] investigated the influence of inlet disturbances on heat transfer in the turbulent flow regime using four different inlet configurations (fully developed with long flow-calming section, bell-mouth, sharp-edged and bend inlet geometries). Heat transfer correlations for turbulent flow were developed as a function of Reynolds number, Prandtl number or axial position, depending on the type of entrance or inlet turbulence.

Mohammed [30] investigated the effect of different levels of hydrodynamically fully developed flow on the laminar heat transfer coefficients. The flow-calming sections had the same tube diameter as the test section (contraction ratio of one) but was unheated, while the test section was heated at a constant heat flux. This generated different velocity distributions in the hydrodynamic entrance region and supressed the inlet effects. In practice, heat exchangers can have different inlet headers that are usually larger than the heat transfer tubes (higher contraction ratios) which affect the heat transfer and pressure drop characteristics. A bell-mouth inlet with a contraction ratio of 3 was also investigated. The local Nusselt numbers for the bell-mouth inlet were found to be higher than for other inlets. This is similar to the findings of Tam and Ghajar [15] where the local heat transfer coefficients were significantly affected by the bell-mouth inlet when compared to the square-edged and re-entrant inlets, especially in the transitional flow regime. Tam and Ghajar [15] also investigated different turbulence levels in the flow-calming section with a bell-mouth inlet geometry by placing different screens close to the end of the flow-calming section (before the bell-mouth inlet). It was found that for finer screens, the turbulence at the bell-mouth inlet was less, which caused an unusual behaviour of the local heat transfer coefficients.

Flow-calming sections are mostly used in convection heat transfer experiments, especially involving the transitional flow regime, to minimize the effect of inlet disturbances on the heat

transfer and pressure drop characteristics in the different flow regimes. Furthermore, flow-calming sections also replicate the heat exchanger inlet header and/or plenums. Different flow-calming section contents have been used in the literature such as plastic straws, honey comb, acrylic plates and different sizes of screens, mostly arranged in a circular tube with a diameter larger than the test section. However, the influence of these contents on the transitional flow regime with different inlet geometries have not yet received attention. Furthermore, these flow-calming sections had different contraction ratios to the test section, similar to the different heat exchanger inlet header/plenum sizes found in many practical applications. Correlations to predict the Reynolds number boundaries of the transitional flow regime as well as the heat transfer coefficients and friction factors in the transitional flow regime are available in the literature [2, 13, 18, 22, 31]. Although most of these correlations distinguish between the different inlet geometries, they do not account for the different contraction ratios. This can change the characteristic behaviour of the entire transitional flow regime and led to inaccurate predictions.

Different flow-calming section diameters with a constant test section diameter would lead to different inlet disturbances, especially with square-edged and re-entrant inlets [2, 11, 18, 22]. Therefore, the purpose of this article is to investigate the effect of contraction ratios together with different inlet geometries on the heat transfer and pressure drop characteristics in the transitional flow regime. To investigate the entire transitional flow regime, results were also given in the laminar and turbulent flow regimes for continuity purposes, because the transitional flow regime is between these two flow regimes.

## 2. Experimental facility

The complete experimental set-up is schematically illustrated in Fig. 1. It has already been described in detail by Meyer et al. [23] and is therefore only succinctly described in this paper. It comprises of a closed fluid loop, flow-calming section and test section. Water was used as the working fluid and was circulated from a 500 $\ell$ storage tank to the flow meters, flow-calming section and test section, and then back to the storage tank for cooling and recirculation. A chiller unit coupled to the storage tank was used to cool down the heated water from the test section to a temperature of approximately 20~22°C, before circulating it through the flow loop again.

A magnetic gear pump with a maximum flow rate of 420 $\ell$/hr was used to circulate the water to the test section and was controlled from a Personal Computer. A voltage signal was sent via a Labview program and data acquisition system (DAQ) to set the required mass flow rate from

the Personal Computer. The pump was connected to the experimental set-up using a rubber hose to prevent any vibration from the pump to the test section. A pressure relief valve was used to bypass the water back to the storage tank when the pressure exceeded the system pressure threshold value. A pressure gauge prior to the flow-calming section was used to monitor the pressure of the system.
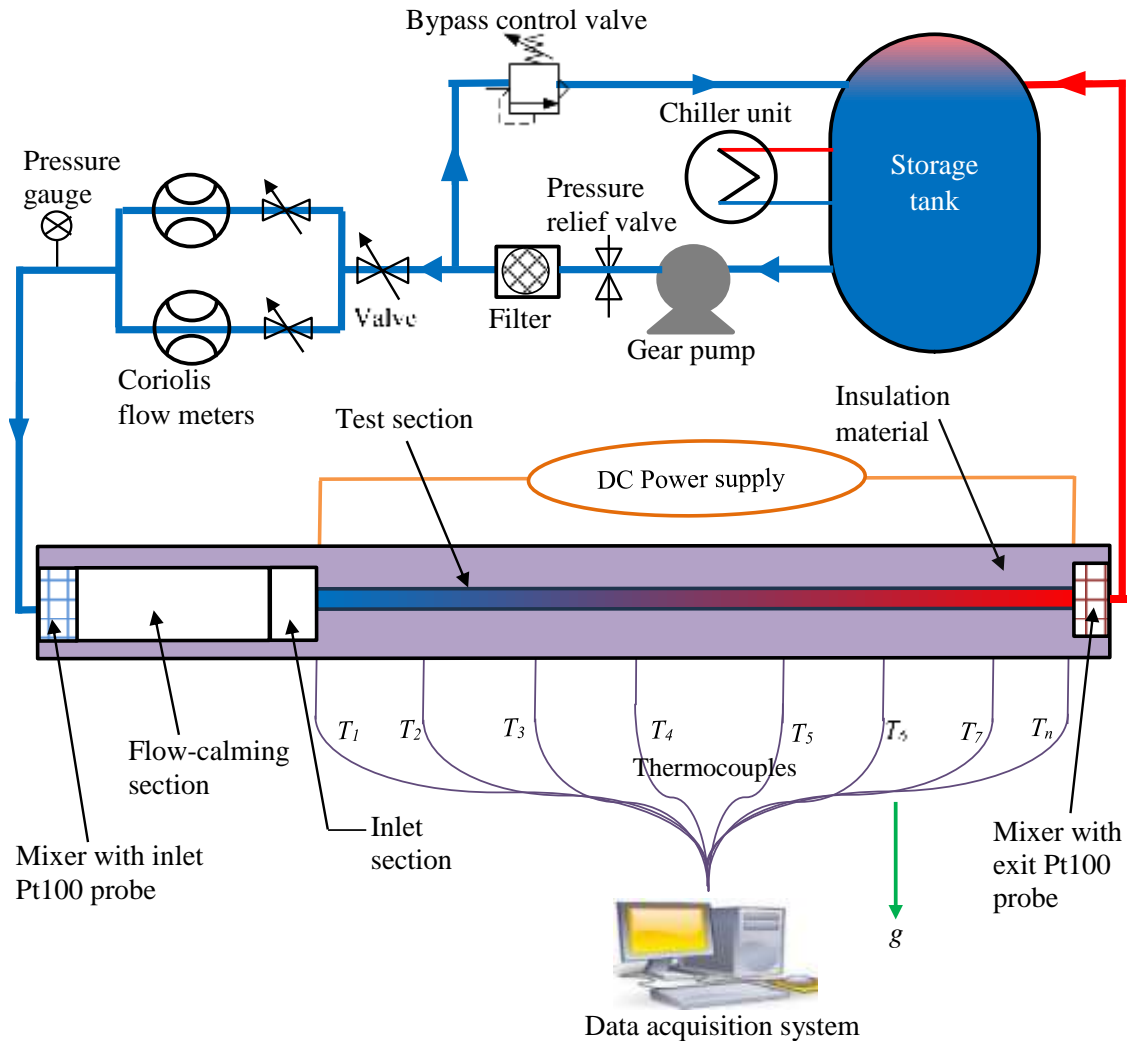


**Fig. 1: Schematic layout of the experimental facility.**

A water bypass line was used to increase the backpressure and to avoid flow pulsations in the test section which might influence the transitional flow regime [32]. Two Coriolis flow meters, with different capacities, were connected in parallel and used to measure the mass flow rate of the water to the test section. The flow meters had an accuracy of ±0.05% of the full scale and a

maximum flow rate of 330 $\ell$/hr and 108 $\ell$/hr, respectively. The flow meter with the higher flow rate (330 $\ell$/hr) was used for measurements in the quasi-turbulent and turbulent flow regimes, while the other mass flow rate meter (108 $\ell$/hr) was used for the laminar to quasi-turbulent flow regimes.

The mixer design of Bakker et al. [33] with alternating right and left hand twisted helical plates, was used for both the inlet and exit mixers. The inlet Pt100 probe was installed inside a soft Nylon mesh downstream of the inlet mixer. The outlet Pt100 probe was also installed just downstream of the outlet mixer with the water stream passing the probe in an axial direction [31].

## 2.1   Flow-calming section and inlet section

Flow-calming sections with different diameters were installed prior to the test section. Fig. 2(a) gives a schematic representation of the original flow-calming section and contents, as used by Ghajar and Tam [2]. The content consisted of plates, straws, screens, etc. and the purpose was to ensure that the flow inlet condition at the test section inlet was uniform and undisturbed. Fig. 2 (b) contains a schematic representation of an empty flow-calming section (except for the inlet mixer) to investigate the effect and significance of the flow-calming section contents on the heat transfer and pressure drop characteristics. Although Fig. 2(a) is shown with a square-edged inlet and Fig. 2(b) with a re-entrant inlet, both types of inlets were tested on calming sections with and without content such as screens, meshes, straws, etc. A hydrodynamically fully developed inlet (Fig. 2(c)), as well as a 90° bend inlet (Fig. 2(d)) typically found in concentric double pipe heat exchangers, respectively, were also investigated for comparison purposes.

The original flow-calming section (Fig. 2(a)) was similar to the flow-calming section of Ghajar and Tam [2] and Tam et al. [18], except that their flow-calming section had a slight change in diameter from the flow-calming section to the inlet section.  To avoid vortex occurrence, the same tube diameter was used for both the flow-calming and inlet sections in this study. The flow-calming sections (Fig. 2(a) and (b)) consisted of a clear acrylic tube with an outer diameter and length of 180 mm and 616 mm respectively, and three air bleed valves were located at the top of the tube to remove any trapped air. The contraction ratio of the original flow-calming section diameter to the test section diameter was 33. Other contraction ratios of 5, 11 and 15 were also investigated by changing the flow-calming section diameter.
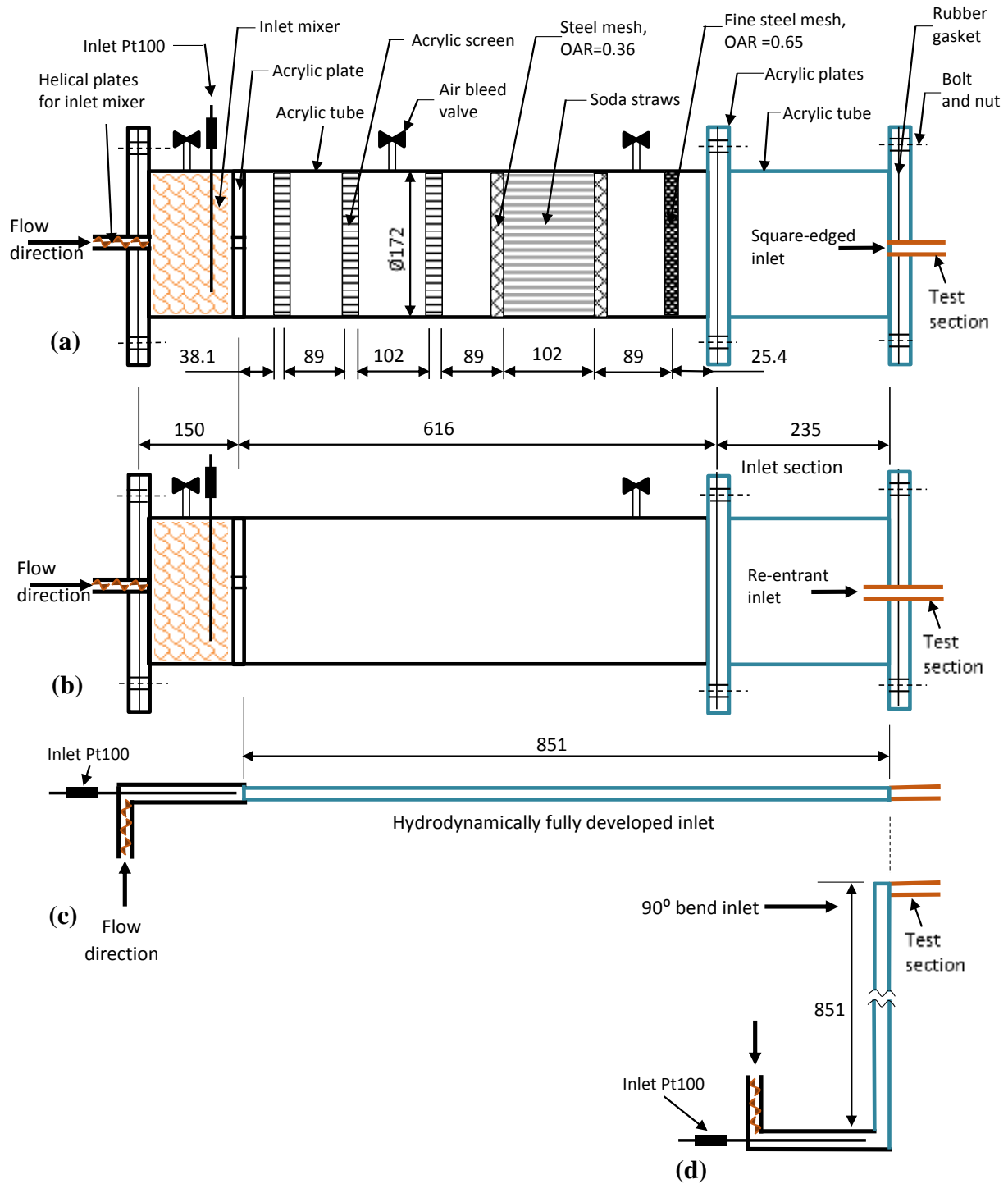
**Fig. 2: Schematic representation of the inlet mixer with (a) the original flow-calming section with a square-edged inlet, (b) the empty flow-calming section a re-entrant inlet, (c) the hydrodynamically fully developed inlet and (d) the 90° bend inlet. (All dimensions given in mm).**

Three perforated acrylic plastic plates, separated at distances of 89 mm and 102 mm, were located 38.1 mm from the flow-calming section inlet. Each acrylic plate had an open area ratio (OAR) of 0.31 and contained 73 holes with a diameter of 11 mm. This was followed by tightly packed plastic straws with an open area ratio of 0.92, length of 102 mm, and diameter of 6 mm. The straws were located 89 mm from the acrylic plates and were placed in-between galvanized steel wire mesh screens with a wire diameter of 0.55 mm and an open area ratio of 0.55. Another fine steel wire mesh screen with a wire diameter of 0.32 mm and open area ration of 0.45 was located approximately 25.4 mm before the outlet of the flow-calming section.

The inlet section containing either the square-edged inlet (Fig. 2 (a)) with sudden contraction or the re-entrant inlet (Fig. 2 (b)) with one diameter slid into the inlet section, was located between the flow-calming section and test section. It consisted of acrylic tube with a length of 235 mm. For a contraction ratio of 33, the outer diameter of the inlet section and the flow-calming section was 180 mm. Both the hydrodynamically fully developed inlet (Fig. 2(c)) and 90° bend inlet (Fig. 2(d)) had the same diameter as the test section (contraction ratio of one) and an isothermal hydrodynamic length equal to the other flow-calming and inlet section length (851 mm). This will ensure that the flow in cases Fig. 2(c) and (d) was fully developed; which will require a length of $125D_i$ based on $L_t = 0.05ReD_i$ and a Reynolds number of 2 500. As lengths of $167D_i$ (851 mm) were used in Fig. 2(c) and (d), hydrodynamic fully developed flow was ensured at the inlet of the heated test section. It was expected that the 90° bend inlet (Fig. 2(d)) would give the maximum disturbance at the entrance of the test section because of the 90º sharp bend and the disturbed velocity distribution at the inlet of the test section.

## 2.2    Test section

Fig. 3 is a schematic representation of the test section used with the four different types of inlets in Fig. 2(a)-(d).  It also indicates the pressure tap locations and thermocouple stations. The test section was made from a smooth hard drawn copper tube with a measured inner and outer diameter of 5.1 mm and 6.3 mm respectively. The test section had a total measured length of 4.6 m and therefore a maximum length-to-diameter ratio ($x/D_i$) of 886. The theoretical thermal entrance length was calculated to be 3.2 m (based on $L_t = 0.05RePrD_i$ using a Reynolds number of 2 100 and a Prandtl number of 6). Therefore, conservatively the last 1.4 m of the test section had fully developed flow and was considered as the "fully developed" part of the test section.  This part of the test section was therefore used to obtain the fully developed results for the pressure drop and

heat transfer measurements. For the temperature measurements the last six stations from stations 16 to 21 were used. Two pressure tap stations (PT-1 and PT-2 with length, $L_{\Delta P}$ as shown in Fig. 3) were located 1 m apart within the fully developed region and corresponded closely to the last six temperature measuring stations, which were 1.05 m apart.
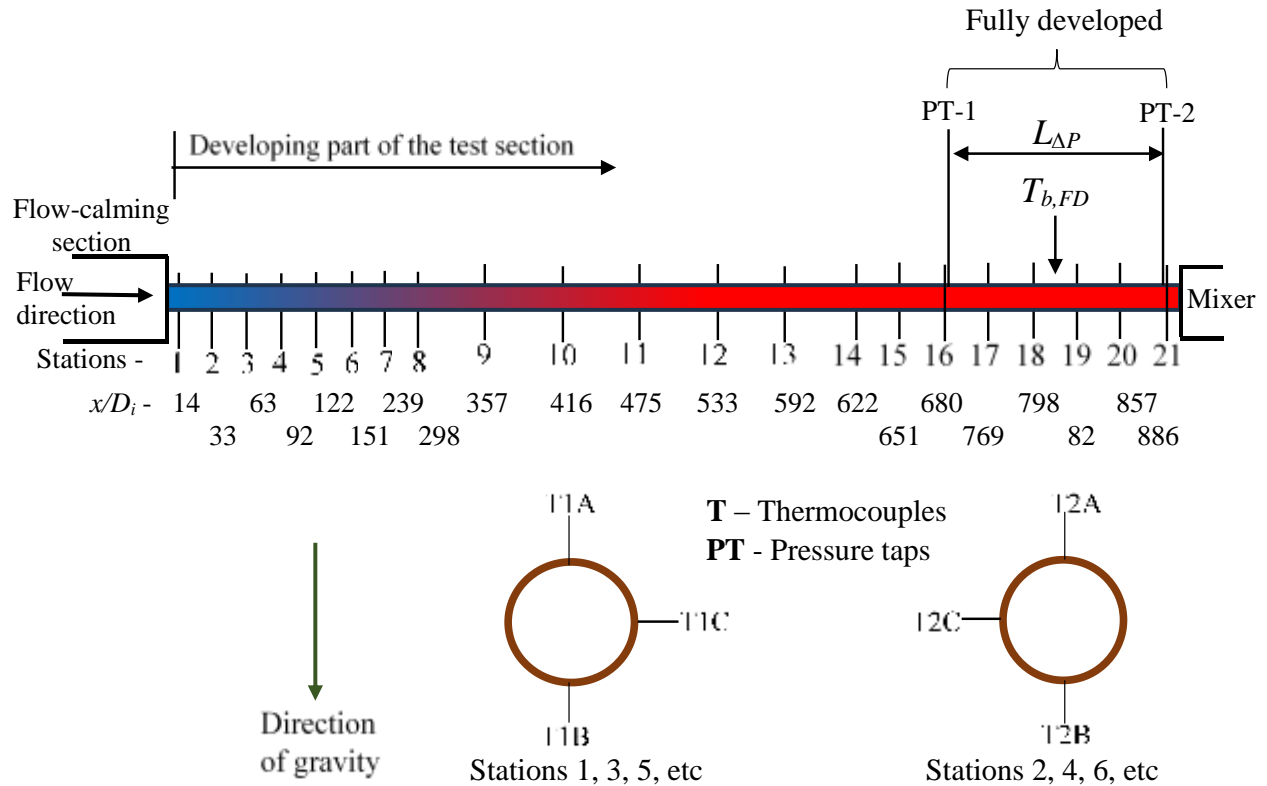


**Fig. 3: Flow directions, pressure taps (PT) and thermocouple stations (T) on the test section. A cross-section of the test section tube shows the thermocouple position per station.**

To ensure that pressure taps did not cause any flow obstructions within the test section, a 0.5 mm diameter hole was drilled through each pressure tap. This hole was less than 10% of the inner diameter of the tube, as suggested by Rayle [34]. A differential pressure transducer with an interchangeable diaphragm was connected to the pressure taps using a Nylon tube. Two different diaphragms were used for the high and low pressure drop measurements. The ranges and accuracies of all the instrumentation used are given in Table 1.

The wall temperatures were measured at 21 thermocouple stations. As shown in Fig. 3, the thermocouple stations were located at closer intervals near the entrance and in the fully developed part to capture enough data in the entrance and fully developed regions. T-type thermocouples

with a diameter of 0.25 mm were used. Due to the small diameter of the test section, three thermocouples were used at each station. One thermocouple at the top and bottom of the tube and another thermocouple alternating at the side between 90° (for station 1, 3, 5, etc.) and 270° (for station 2, 4, 6, etc.). The thermocouples were soldered to the outer wall of the tube by drilling a 0.4 mm depression and inserting a flux and solder.

**Table 1: Ranges and accuracies of the instrumentation used.**

| Instruments | Range | Accuracy |
|---|---|---|
| DC power supply | 0 – 1 500 W | 3 W |
| Pt100 probes | 0 – 100°C | 0.06°C |
| Thermocouples | -200 – 350°C | 0.1°C |
| Pressure transducers | 0 – 3.5 kPa | 8.75 Pa |
| | 0 – 14 kPa | 35 Pa |
| | | |
| Coriolis flow meters | | |
| CMFS010 | 0 – 108 ℓ/hr | 0.054 ℓ/hr |
| CMFS015 | 0 – 330 ℓ/hr | 0.165 ℓ/hr |

For a constant heat flux boundary condition, two T-type constantan heating wires, with diameters of 0.38 mm, were tightly coiled around the test section (skipping the thermocouple junctions) and connected in parallel to the DC power supply. The two heating wires were connected in opposite polarities to avoid electromagnetic interferences due to the applied currents [32].

**2.3 Insulation**

The flow-calming section, inlet section, test section, mixers and tubes were insulated to prevent heat transfer to the environment using insulation material with a thermal conductivity of 0.034 W/m K. The thickness of the insulation around the test section was 60 mm and the maximum heat loss was estimated with one-dimensional heat transfer calculations (taking into consideration the average measured wall and outside insulation temperature measurements and insulation resistance) to be less than 2%.

**2.4 Experimental procedure**

Steady-state conditions were reached two hours after the first start-up of a day. Steady-state conditions were assumed once there were no significant changes in the mass flow rates, temperatures, currents, pressure drops and energy balance readings. The experiments were conducted by starting with the highest mass flow rate and then decreasing the mass flow rates by
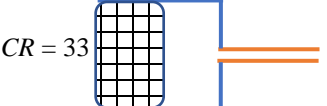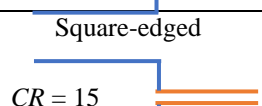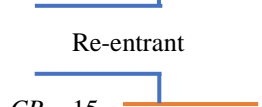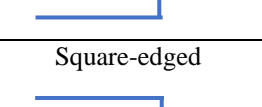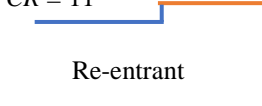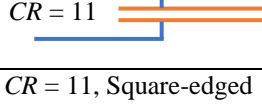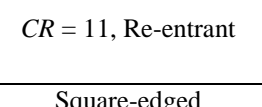
adjusting the pump speed in the Labview program. To minimize flow pulsations, the bypass and supply valves were continuously adjusted suc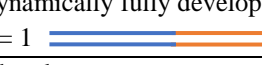h that the pump can operate at higher mass flow rates. The heat flux was set from the DC power supply by applying the required voltage and current signals.

Measurements were taken at greater mass flow rate intervals in the laminar and turbulent flow regimes, but at closer intervals near and within the transitional flow regime. After each Reynolds number increment, approximately 5-10 minutes in the quasi-turbulent and turbulent flow regimes and 15-20 minutes in the laminar flow regime, were required to reach steady-state. In the transitional flow regime, fluctuations in temperature, mass flow rate, pressure drop and energy balances were observed, therefore more time (approximately 20-30 minutes) was required to reach steady-state conditions [11]. Once steady-state conditions were achieved, 400 data points were logged at a frequency of 20 Hz. These data points were then averaged to obtain one data point. The data logged included the inlet and exit temperatures, wall temperatures, ambient temperatures, mass flow rates and pressure drops. The temperature of the water in the storage tank was also monitored to ensure a constant inlet temperature. All the data obtained were saved and exported to a separate program for the data analysis.

## 2.5    Experimental test matrix

Table 2 summarizes the experiments that were conducted using different flow-calming sections, contraction ratios (ratios of flow-calming section inner diameters and test section inner diameters) and inlet types. As the focus of this study was on transitional flow regime, experiments were only conducted between Reynolds numbers of 1 000 and 6 000. This ensured that the entire transitional flow regime was covered, as well as sufficient parts of the laminar and quasi-turbulent flow regimes for continuity, without getting to high water outlet temperatures (laminar flow) or high heat transfer coefficient uncertainties (turbulent flow).

**Table 2: Experimental test matrix. Red indicates heating of the test section while blue identifies part of the flow-calming section without heating**

| Calming section | Contraction ratio (CR) and inlet type | Heat flux [kW/m²] | Reynolds number | Mass flow rate measurements | Temperature measurements | Pressure drop measurements |
|---|---|---|---|---|---|---|
| Original | Square-edged | 0 | 1 047 – 6 014 | 40 | 2 600 | 40 |
| | | 4 | 1 091 – 5 826 | 37 | 2 405 | 37 |
| | $CR = 33$ | 6 | 1 451 – 6 082 | 36 | 2 340 | 36 |
| | | 8 | 1 946 – 5 886 | 34 | 2 210 | 34 |
| Empty | Square-edged | 0 | 1 045 – 5 706 | 39 | 2 535 | 39 |
| | | 4 | 1 261 – 5 253 | 34 | 2 210 | 34 |
| | $CR = 33$ | 6 | 1 592 – 5 749 | 33 | 2 145 | 33 |
| | | 8 | 2 081 – 5 840 | 32 | 2 080 | 32 |
| | Re-entrant | 0 | 1 084 – 5 428 | 44 | 2 860 | 44 |
| | | 4 | 1 075 – 5 568 | 35 | 2 275 | 35 |
| | $CR = 33$ | 6 | 1 486 – 5 782 | 32 | 2 080 | 32 |
| | | 8 | 1 906 – 5 583 | 30 | 1 950 | 30 |
| Empty | Square-edged | 0 | 1 015 – 5 259 | 36 | 2 340 | 36 |
| | | 4 | 1 219 – 5 691 | 35 | 2 275 | 35 |
| | $CR = 15$ | 6 | 1 546 – 5 868 | 33 | 2 145 | 33 |
| | | 8 | 2 017 – 5 848 | 32 | 2 080 | 32 |
| | Re-entrant | 0 | 1 131 – 5 223 | 36 | 2 340 | 36 |
| | | 4 | 1 220 – 5 433 | 34 | 2 210 | 34 |
| | $CR = 15$ | 6 | 1 551 – 5 814 | 34 | 2 210 | 34 |
| | | 8 | 2 061 – 5 913 | 33 | 2 145 | 33 |
| Empty | Square-edged | 0 | 1 098 – 5 705 | 37 | 2 405 | 37 |
| | | 4 | 1 211– 5 676 | 35 | 2 275 | 35 |
| | $CR = 11$ | 6 | 1 451 – 5 899 | 34 | 2 210 | 34 |
| | | 8 | 1 977 – 5 915 | 33 | 2 145 | 33 |
| | Re-entrant | 0 | 1 038 – 5 121 | 38 | 2 470 | 38 |
| | | 4 | 1 211 – 5 717 | 34 | 2 210 | 34 |
| | $CR = 11$ | 6 | 1 475 – 5 655 | 35 | 2 275 | 35 |
| | | 8 | 2 059 – 5 884 | 33 | 2 145 | 33 |
| Original | $CR = 11$, Square-edged | 0 | 1 026 – 5 032 | 36 | 2 340 | 36 |
| | | 8 | 2 065 – 5 900 | 34 | 2 210 | 34 |
| | $CR = 11$, Re-entrant | 0 | 1 131– 5 428 | 37 | 2 405 | 37 |
| | | 8 | 2 019 – 5 859 | 30 | 1 950 | 30 |
| Empty | Square-edged | 0 | 1 079 – 4 853 | 33 | 2 145 | 33 |
| | | 4 | 1 092 – 5 354 | 33 | 2 145 | 33 |
| | $CR = 5$ | 6 | 1 451 – 5 573 | 33 | 2 145 | 33 |
| | | 8 | 2 007 – 5 759 | 32 | 2 080 | 32 |
| | Re-entrant | 0 | 1 032 – 5 164 | 37 | 2 405 | 37 |
| | | 4 | 1 173 – 5 349 | 34 | 2 210 | 34 |
| | $CR = 5$ | 6 | 1 477 – 5 196 | 32 | 2 080 | 32 |
| | | 8 | 2 000 – 5 250 | 31 | 2 015 | 31 |
| Empty | Hydrodynamically fully developed | 0 | 1 051 – 5 427 | 41 | 2 665 | 41 |
| | $CR = 1$ | 8 | 1 866 – 5 886 | 36 | 2 340 | 36 |
| Empty | 90º bend | 0 | 1 069 – 5 144 | 43 | 2 795 | 43 |
| | $CR = 1$ | 8 | 1 865 – 5 870 | 38 | 2 470 | 38 |

| | | | | |
|---|---|---|---|---|
| Total | | 1 538 | 99 970 | 1 538 |

A total of 1 538 mass flow rate measurements, 99 970 temperature measurements and 1 471 pressure drop measurements were conducted. "Original" in Table 2 refers to the flow-calming section with full contents (such as shown in Fig. 2(a)) while "Empty" refers to the flow-calming section without contents on the inside (such as shown in Fig. 2(b)).

## 2.6  Data reduction

Over the tube with measured length, $L$, the fluid temperatures, $T(x)$, at any axial position, $x$, were determined from the measured inlet, $T_i$, and exit, $T_e$, fluid temperatures as obtained from the two Pt100 probes located at the inlet and outlet of the test section:

$$T(x) = T_i + \frac{(T_e - T_i)x}{L} \tag{1}$$

Thus, linear temperature profiles were assumed for the temperatures as constant heat fluxes were applied to the test section. The bulk temperature for the fully developed part of the test section, ($T_{b,FD}$ in Fig. 3), could therefore be determined from the measured distance $x = 3.92$ m from the inlet as shown in Fig. 3. Depending on what was required (fully developed bulk values or local values) these temperatures were also used to determine all the fluid properties (densities, $\rho$, viscosities, $\mu$, Prandtl numbers, $Pr$, specific heat values, $C_p$, and volume expansion coefficients, $\beta$) using the correlations of Popiel and Wojtkowiak [35] for water.

The friction factors, $f$, were obtained from the calculated frictional pressure drops, $\Delta P_f$, as follows:

$$f = \frac{\Delta P_f \rho_{b,FD} \, \pi^2 D_i^{\,5}}{8 L_{\Delta P} \dot{m}^2} \tag{2}$$

The measured tube inner diameter, $D_i$, was 5.1 mm, the measured distance, $L_{\Delta P}$, between the two pressure taps was 1 m, and the mass flow rates, $\dot{m}$, were obtained from the mass flow rate measurements.

The local or bulk fully developed Reynolds numbers were calculated from the measured mass flow rates:

$$Re = \frac{4\dot{m}}{\pi D_i \mu} \tag{3}$$

with the viscosities, $\mu$, determined at the local mean fluid temperature, $T(x)$, or at the bulk fully developed, $b,FD$ temperature station as shown in Fig. 3.

The heat transfer rates, $\dot{Q}_f$, to the fluid were determined from the measured mass flow rates, $\dot{m}$, and the difference between the measured inlet and exit fluid temperatures:

$$\dot{Q}_f = \dot{m} C_p (T_e - T_i) \tag{4}$$

The energy balance error, $eb$, was used to compare the measured heat transfer to the water, $\dot{Q}_f$, with the electrical energy supplied, $\dot{Q} = IV$, and is given as:

$$eb = \left[ \frac{\dot{Q} - \dot{Q}_f}{\dot{Q}} \right] \times 100 \tag{5}$$

where $I$ and $V$, were the measured currents and voltage drops.

The heat flux applied to the fluid, $\dot{q}_f$, was calculated as follows:

$$\dot{q}_f = \frac{\dot{Q}_f}{\pi D_i L} \tag{6}$$

The heat transfer rate to the fluid, $\dot{Q}_f$, was used to determine the heat flux rather than the electrical power supplied, $\dot{Q}$, as the electrical power supplied was always a little larger than the heat transfer rate to the water, $\dot{Q}_f$, because of the heat losses from the test section. These heat losses were on average 2.5% and corresponded well to the theoretical heat losses that were calculated based on the resistance of the insulation material, average measured wall temperatures and measured temperatures on the outside of the insulation wall.

The local heat transfer coefficients at any axial point, $x$, from the tube inlet were determined as:

$$h = \frac{\dot{q}_f}{T_{iw} - T(x)} \tag{7}$$

where $T(x)$ was obtained from Eq. (1) and $T_{iw}$ was the inner wall temperature obtained by taking into consideration the tube thermal resistance, $R_w$, as:

$$T_{iw} = T_{ow} - \dot{Q}_f R_w \tag{8}$$

The outside wall temperatures, $T_{ow}$, were obtained from the wall temperature measurements at each station and were the average of the three thermocouple measurements at each station. The tube thermal resistance, $R_w$, was determined as:

$$R_w = \frac{ln(D_o/D_i)}{2\pi k_{Cu} L} \tag{9}$$

where $D_o$ (6.3 mm) and $D_i$ (5.1 mm) were the measured tube outer and inner diameters and $k_w$ the thermal conductivity of the copper tube which was 401 W/m.K [20].

These calculations showed that the temperature differences between the inside and outside walls were negligible and much smaller than the errors of the thermocouple measurements. Although these differences were taken into consideration in this study, for all practical purposes it could be assumed that the inner wall temperatures were equal to the measured outside wall temperatures.

From the local heat transfer coefficients, the local Nusselt numbers were calculated as:

$$Nu = \frac{hD_i}{k} \tag{10}$$

The average Nusselt numbers of the fully developed part of the test section from $x = 3.47$ m (station 16 in Fig. 3) to $x = 4.52$ m (station 21) were obtained from calculating the average of the local Nusselt numbers at the last six measuring station.

Also determined were the Colburn $j$-factors:

$$j = \frac{Nu}{RePr^{\frac{1}{3}}} \tag{11}$$

and the Grashof number, $Gr$:

$$Gr = \frac{g\beta\rho^2\left(T_w - T(x)\right){D_i}^3}{\mu^2} \qquad (12)$$

as well as the modified bulk Grashof number, $Gr^*$, in terms of heat flux:

$$Gr^* = \frac{g\beta\rho^2 \dot{q}_f {D_i}^4}{k\mu^2} \qquad (13)$$

The Rayleigh number, $Ra$, was determined from the product of the Grashof number and Prandtl number:

$$Ra = GrPr \qquad (14)$$

The average values of the Grashof numbers and Rayleigh numbers over the fully developed part of the test section were determined by averaging the last six values.

The Reynolds number at the start of the transitional flow regime, $Re_{cr,}$ as recently defined by Everts and Meyer [11], was obtained as:

$$Re = Re_{cr} \text{ when: } \left(\frac{dj}{dRe}\right)_{i-2:i} = 0 \qquad (15)$$

where $i$-2:$i$ means that at any given point $i$, $dj/dRe$ was determined from the three data points at $Re(i$-2$)$, $Re(i$-1$)$ and $Re(i)$ for increasing Reynolds numbers. While the Reynolds number at the end of the transitional flow regime, $Re_{qt,}$ was defined as [36]:

$$Re = Re_{qt} \text{ when: } \left(\frac{d^2Nu}{dRe^2}\right)_{i:i+2} \geq -0.00015 \qquad (16)$$

where $i$:$i + 2$ means that at any given point $i$, $dNu/dRe$ was determined from the three data points at $Re(i)$, $Re(i+1)$ and $Re(i+2)$ for increasing Reynolds numbers (while Eq. (15) used the results at the previous two Reynolds numbers).

**2.7 Uncertainty**

All uncertainties were estimated within a 95% confidence level as prescribed by Dunn [37]. For the uncertainty analyses of this paper, the manufacturer instrumentation errors were used as the fixed errors and two times the standard deviation of 400 data points as the random error. The thermocouples and Pt100 probes were calibrated against a reference thermometer with an accuracy of ±0.03°C. The maximum Reynolds number uncertainty was found to be approximately 1.4%. The maximum friction factor uncertainty in the laminar flow regime was 8% and reduced to approximately 2% in the turbulent flow regime. In the transitional flow regime, the friction factor uncertainty increased to a maximum of 12%. This was due to fluctuations of the mass flow rates, temperatures and pressure drop measurements within the transitional flow regime [11].

The maximum Colburn $j$-factor uncertainties were 3%, 13%, and 6% respectively in the laminar, transitional and turbulent flow regimes. Again, the higher uncertainties in the transitional flow regime were caused by the higher fluctuations in the wall and exit temperature measurements. All these uncertainties were for the original flow-calming section with the maximum contraction ratio of 33 (Fig. 2(a)) and the maximum heat flux of 8 kW/m². For all the contraction ratios (both empty and original flow-calming sections) used in this study, the uncertainties followed a similar trend in each flow regime. Furthermore, the re-entrant and square-edged inlets showed no significant difference in the uncertainties. However, as the heat flux decreased from 8 kW/m² to 4 kW/m², the heat transfer uncertainties increased slightly, as expected, due to the decrease in the temperature difference between the bulk fluid and wall temperatures. For the lowest heat flux of 4 kW/m², the maximum Colburn $j$-factor uncertainties were 4%, 18%, and 12% respectively, in the laminar, transitional and turbulent flow regimes.

Although the experiments were conducted at Reynolds numbers up to 6 000, the results showed that for this paper, sufficient conclusions could be made for Reynolds numbers up to 4 000. At this Reynolds number the maximum Colburn $j$-factor uncertainties in the turbulent flow regime were 4.4%. It has also been found that the Nusselt number uncertainties were for all practical purposes the same as that of the Colburn $j$-factors uncertainties.

**2.8 Validation**

Validation experiments were conducted using the original flow-calming section with a maximum contraction of ratio of 33. The validation experiments consisted of isothermal friction factors, local laminar Nusselt numbers for forced and mixed convection conditions and average

Colburn *j*-factors in the turbulent flow regime. The detailed validation of the experimental results can be found in Meyer et al. [23] and a summary of the important conclusions are given in this paper.

### 2.8.1 Isothermal pressure drop

The laminar isothermal friction factors compared well with the Poiseuille [38] correlation between Reynolds numbers of 1 000 and 2 200 with an average deviation of 2.7% and a maximum deviation of 5%. In the turbulent flow regime, the experimental data compared well with the Blasius [39] correlation between Reynolds number of 4 000 and 6 000, with an average deviation of 1% and a maximum deviation of 1.7%.

### 2.8.2 Heat transfer

At a heat flux of 280 W/m$^2$, the local laminar Nusselt numbers converged to the theoretical forced convection Nusselt of 4.36 for a constant heat flux boundary condition at a bulk Reynolds number of 660 and bulk Prandtl number of 5.18. According to the newly developed flow regime map of Everts and Meyer [11], the flow at these conditions was expected to be dominated by forced convection. The flow was fully developed from $x/D = 416$ and the average Nusselt number for the fully developed flow between $x/D = 416$ and $x/D = 857$ was 4.39, which is within 0.7% of the value of 4.36.

The local Nusselt numbers at a heat flux of 6 kW/m$^2$, bulk Prandtl number of 3.29 and bulk Reynolds number of 1 450, were compared with the correlations of Meyer and Everts [7] and Morcos and Bergles [40]. According to the flow regime map of Everts and Meyer [11], the flow was expected to be dominated by mixed convection which was confirmed by the measurements which produced Nusselt numbers much higher than 4.36. Furthermore, the results also correlated well with the correlation of Meyer and Everts [7] with an average deviation of 4% and maximum deviation of 8%.

Although the correlation of Morcos and Bergles [40] was developed for tube wall parameters, $P_w = kD_i/(k_w t)$, between 2 and 66, it varied in this study between 0.0133 and 0.0138, which was far outside the specified range for which the correlation was developed. However, the average deviation between the experimental results and the correlation of Morcos and Bergles was 2.6%, and the maximum deviation was only 5%. It therefore seemed as if the correlation of Morcos and Bergles were valid for a much wider range of tube wall parameters than they have specified. This was also found by Meyer and Everts [7].

The average Colburn *j*-factors in the turbulent flow regime compared well with the correlation of Gnielinski [41] and the newly developed correlation of Meyer et al. [42] with average deviations of 6.1% and 5.6% respectively and maximum deviations of 13% and 8.6% respectively. The deviation between the experimental results and literature were larger in the turbulent flow regime than in the laminar flow regimes. This was as expected, because the temperature differences between the wall and fluid decreased with increasing Reynolds number, which led to increased uncertainties.

## 3. Results

### 3.1 Calming section content

To investigate the effect of different content inside a flow-calming section the heat transfer and pressure drop characteristics of the original flow-calming section (Fig. 2(a)) was compared to an empty flow-calming section (Fig. 2(b)) using two different contraction ratios. The flow-calming section diameters were 170 mm and 56 mm, leading to contraction ratios of 33 and 11. All the flow-calming and inlet sections were of the same length.

### 3.1.1 Pressure drop characteristics

Fig. 4(a) and (b) show the friction factor results for the original and empty flow-calming sections (as shown in Fig. 2) with contraction ratios of 11 and 33 respectively and a square-edged inlet geometry. Also included are $f = 64/Re$ and the Blasius [39] correlations. For both contraction ratios (Fig. 4(a) and (b)), the results showed no significant difference between the two flow-calming sections in all the flow regimes. For each contraction ratio, transition occurred at approximately the same critical Reynolds number. For the contraction ratio of 11 (Fig. 4(a)), the critical Reynolds numbers at which transition started were 2 300 and 2 280 for the empty and original flow-calming section respectively, while for the contraction ratio of 33 (Fig. 4(b)) it was 2 218 and 2 200 respectively. Similarly, Fig. 4 indicates that transition ended at approximately the same Reynolds numbers for both flow-calming sections.

Fig. 4(c) and (d) compares the isothermal friction factors of the original and an empty flow-calming sections with a re-entrant inlet and a contraction ratio of 11 and 33 respectively. Similar to the square-edged inlet, the flow-calming section content had a negligible influence on the friction factors in all the flow regimes and transition occurred at approximately the same Reynolds numbers.
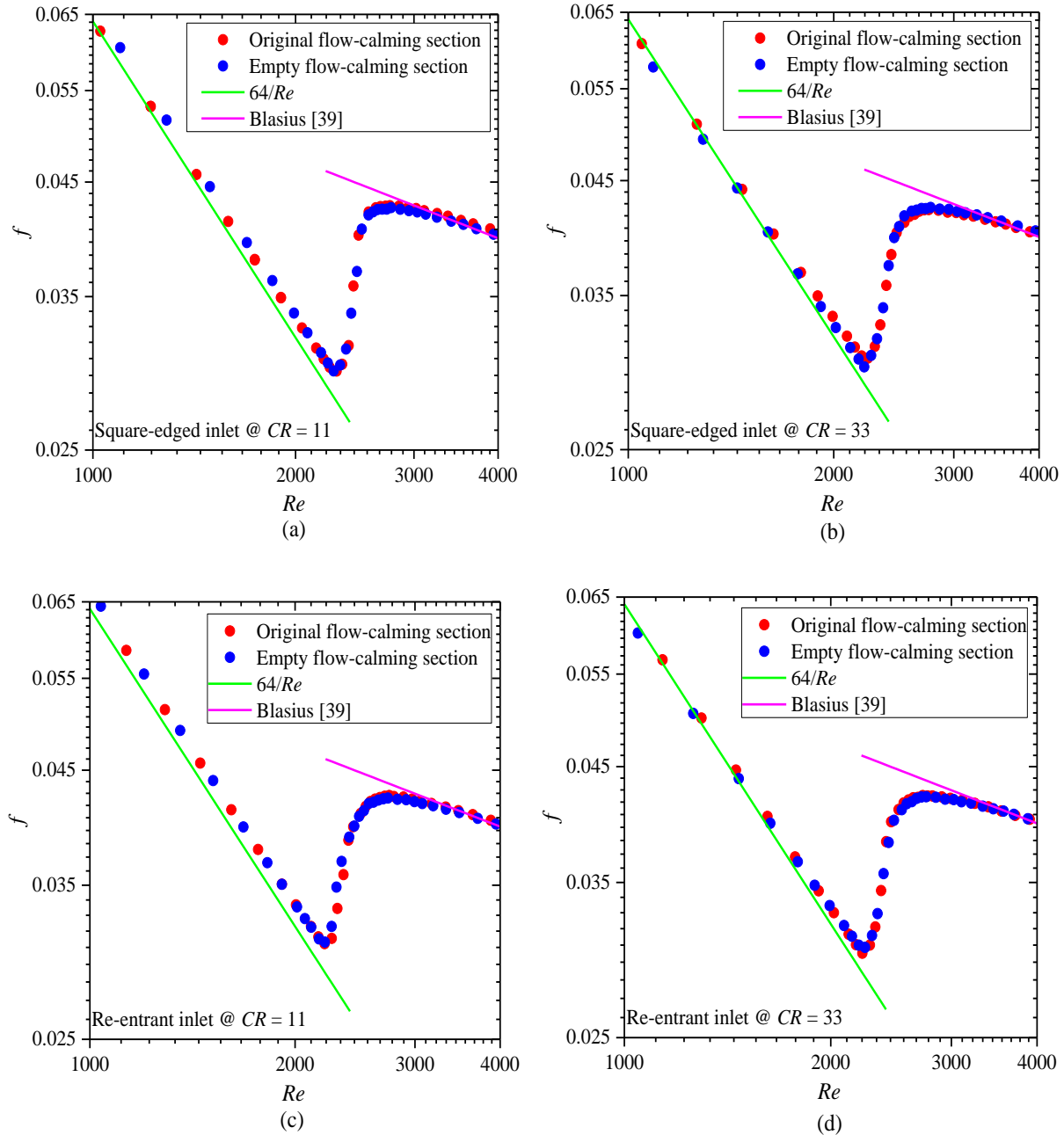
**Fig. 4: Comparison of isothermal friction factors as a function of Reynolds number using the original and empty flow-calming sections with a square-edged inlet and contraction ratios, *CR*, of (a) 11 and (b) 33, and also with a re-entrant inlet for contraction ratios of (c) 11 and (d) 33.**

It was therefore concluded that the flow-calming section contents had no influence on the isothermal friction factors in all flow regimes, or on the boundaries of transitional flow regime, when square-edged and re-entrant inlets were used. Although it was not shown in this paper,

similar results and conclusions were found for the diabatic friction factors at different heat fluxes of 4, 6 and 8 kW/m$^2$.

### 3.1.2   Heat transfer characteristics

Fig. 5 compares the heat transfer coefficients in terms of the Colburn $j$-factors as a function of Reynolds numbers for the different flow-calming sections, contraction ratios and inlet geometries at a heat flux of 8 kW/m$^2$, specifically for the fully developed part (indicated in Fig. 3) of the test section between thermocouple stations 16 to 21 ($680 \leq x/D_i \leq 886$). This was the maximum heat flux tested with the lowest uncertainties. Similar to the friction factor results, Fig. 5 indicates that the flow-calming section contents had no influence on the Colburn $j$-factors in all the flow regimes when square-edged (Fig. 5(a) and ((b)) and re-entrant (Fig. 5(c) and ((d)) inlet geometries were used. Furthermore, transition also started and ended at approximately the same Reynolds numbers. It was expected that the same conclusions could be made from the friction factor and Colburn $j$-factor results, because Everts and Meyer [7] showed that a direct relationship between pressure drop and heat transfer existed in the transitional flow regime.

A possible reason for the negligible difference might be that the effects of the flow-calming section contents diminished in the empty inlet section between the flow-calming section and the test section (the length of this section might be a contributing factor). Tam and Ghajar [15] found that different screen sizes placed near the outlet of the flow-calming section had a significant influence on the local heat transfer coefficients when a bell-mouth inlet was used. The reason for this was because of the bell-mouth geometry that gradually contracts from the flow-calming section (close to the screen) to the inlet of the test section. This caused the disturbances caused by the screens to be transferred to the test section, unlike the square-edged and re-entrant inlets where these disturbances were suppressed in the inlet section.

Although it is not shown in this paper, similar results and conclusions were found with the other heat fluxes of 4 and 6 kW/m$^2$ and contraction ratios of 11 and 33, where the flow-calming section contents had no influence on the heat transfer coefficients in all the flow regimes using square-edged and re-entrant inlets.
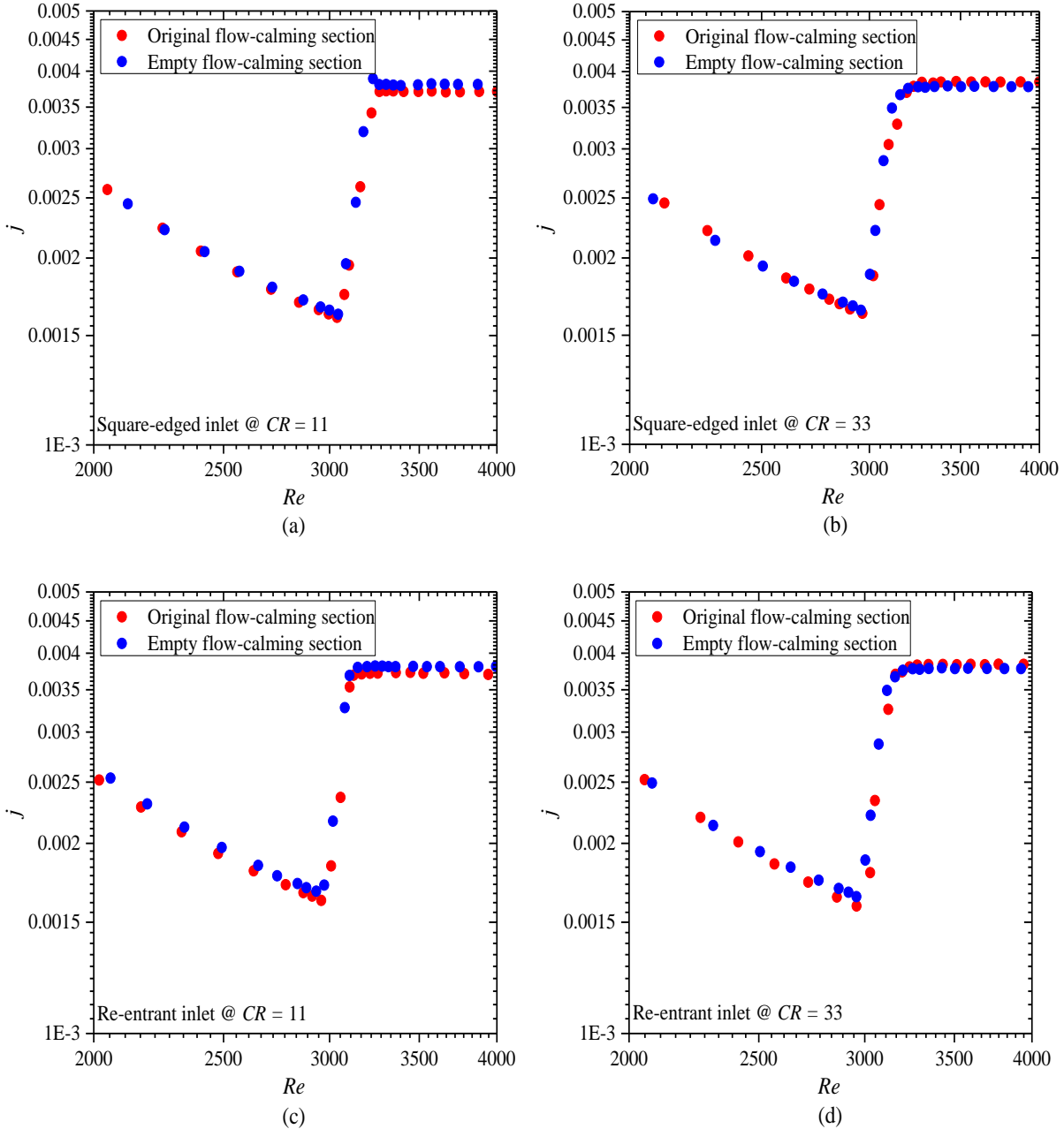
23

**Fig. 5: Comparison of the fully developed Colburn *j*-factors as a function of Reynolds number for the original and empty flow-calming sections at a heat flux of 8 kW/m² for (a) square-edged with a contraction ratio of 11, (b) square-edged with a contraction ratio of 33, (c) re-entrant with a contraction ratio of 11 and (d) re-entrant with a contraction ratio of 33.**

## 3.2    Contraction ratio

Heat exchangers in practice have different contraction ratios, depending on the type and size of the inlet header or plenum geometry. This may lead to different levels of inlet disturbances that could influence the start and end of the transitional flow regime. It was concluded in Sections 3.1.1 and 3.1.2 that the content of the flow-calming section had no influence on the pressure drop and

24

heat transfer characteristics for square-edged and re-entrant inlet geometries. An empty flow-calming section was therefore used to investigate the effect of contraction ratio, because it was challenging to construct a long flow-calming section with a small tube diameter of less than 26 mm, using the same flow-calming section contents and arrangements as in Fig. 2(a). Four different contraction ratios (5, 11, 15 and 33), with equal flow-calming and inlet section lengths, were compared using square-edged and re-entrant inlets. A hydrodynamically fully developed inlet (Fig. 2(c)) and a 90° bend inlet (Fig. 2(d)) were also used for comparison purposes. The analysis involved both isothermal and diabatic flow conditions in order to compare the effect of heating on the different contraction ratios.

### 3.2.1  Pressure drop characteristics

Fig. 6 shows the fully developed isothermal and diabatic friction factors for the different contraction ratios using the square-edged and re-entrant inlet geometries. Also included are the results for the hydrodynamically fully developed (empty black circles) and the 90° bend (stars) inlets. Similar to the results obtained in the previous studies [2, 9, 13, 17, 22] that investigated different inlet geometries, Fig. 6 indicates that the friction factors in the laminar and quasi-turbulent flow regimes were unaffected by the contraction ratio. The isothermal friction factors (Fig. 6(a) and (b)) correlated well with the $f = 64/Re$ and Blasius [39] correlations, but the laminar diabatic friction factors were significantly higher than $f = 64/Re$ due to buoyancy effects [7, 13, 23]. However, the isothermal and diabatic friction factors in the transitional flow regime of both inlet geometries were affected. For the square-edged inlet in Fig. 6(a) and (c), transition was delayed as the contraction ratio decreased from 33 to 5.
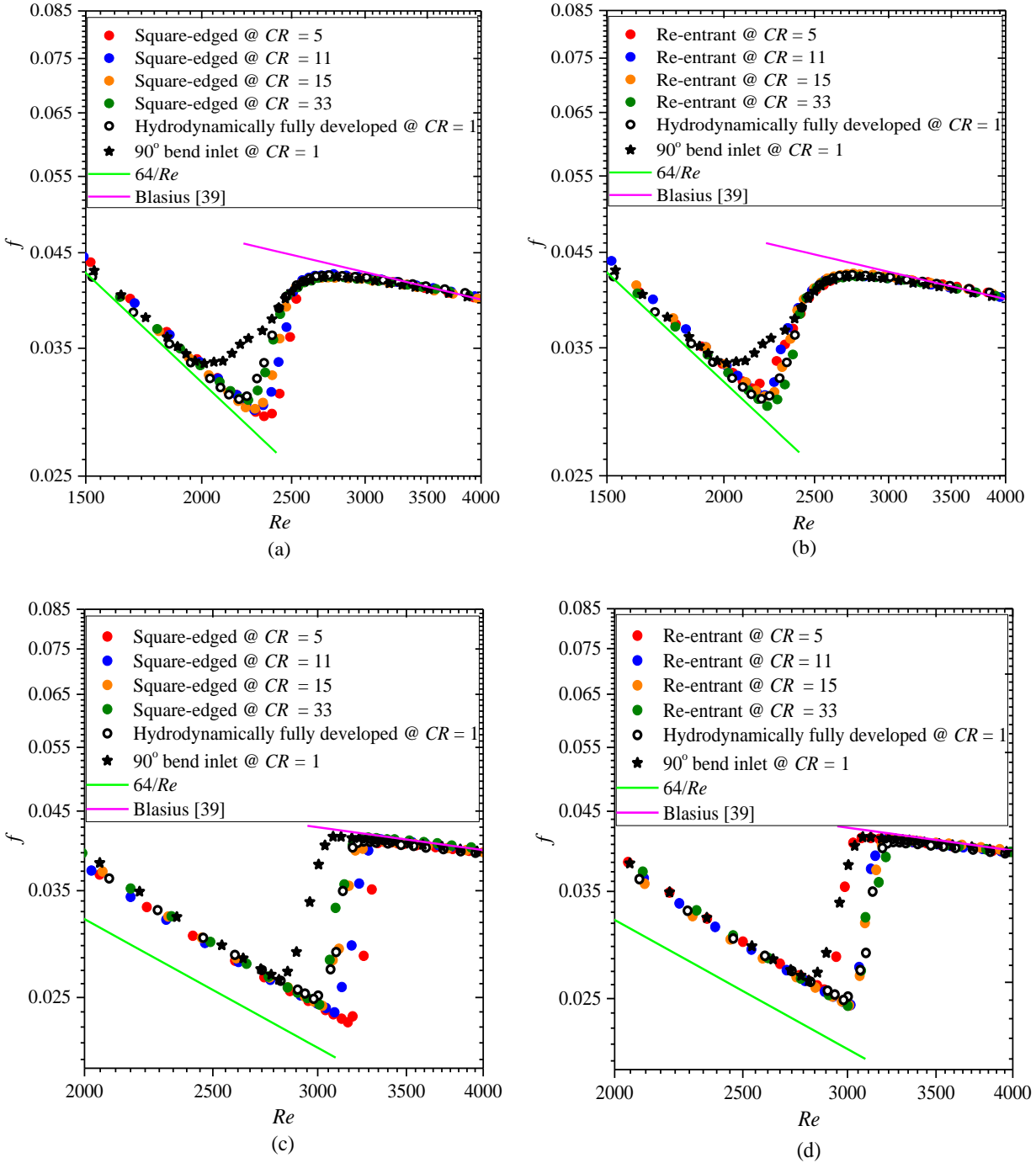
**Fig. 6: Comparison of isothermal friction factors for (a) a square-edged and (b) a re-entrant inlet, as well as diabatic friction factors at a heat flux of 8 kW/m² for (c) a square-edged and (d) a re-entrant inlet, as a function of Reynolds number.**

This explains why Olivier and Meyer [22] found a delay in transition for the isothermal friction factors when the contraction ratio decreased from 9.6 to 7.3 due to different test section diameters (15 mm and 19 mm) with the same flow-calming section and a square-edged inlet. The protrusion of the tube into the inlet section by one-diameter for the re-entrant inlet (Fig. 2 (b)) led

to increased inlet disturbances when compared to the square-edged inlet. This caused transition to occur much earlier for the re-entrant inlet (Fig. 6 (b) and (d)) than the square-edged inlet (Fig. 6 (a) and (c)) as was also found by Ghajar and Tam [2, 13, 15, 17] and Olivier and Meyer [22]. Fig. 6 (b) and (d) also indicate that for a re-entrant inlet, transition was delayed for increasing contraction ratios, which is opposite than what was found for the square-edged inlet. Furthermore, due to the increased disturbance caused by the tube protrusion of the re-entrant inlet, the effect of the contraction ratio was less than for the square-edged inlet. The inlet disturbances caused by tube protrusion decreased with increasing contraction ratio, which explains why transition was delayed. From Fig. 6 (c) and (d) it follows that the difference between the diabatic friction factors in the transitional flow regime for contraction ratios of 15 and 33 were small. It can therefore be assumed that there will be a negligible difference between the transitional flow friction factors of higher contraction ratios.

Fig. 6 indicates that the hydrodynamically fully developed inlet results were similar to the results obtained using the maximum contraction ratio of 33 for both the square-edged and re-entrant inlets. This means that as the contraction ratios increased and approached infinity, the effects of the inlet disturbances on the transitional flow regime became negligible and results approached those of the hydrodynamically fully developed inlet. However, as the contraction ratio decreased and approached 1, transition was significantly affected (especially at lower contraction ratios between 5 and 1), and was significantly delayed for the square-edged inlet and occurred much earlier for the re-entrant inlet. As expected, transition occurred earlier for the 90° bend inlet than for the other inlets and contraction ratios because of the significantly high inlet disturbances generated by the 90° bend at the inlet.

### 3.2.2 Heat transfer characteristics

Fig. 7 compares the heat transfer results in terms of the Colburn $j$-factors for different inlet geometries and contraction ratios at a constant heat flux of 8 kW/m². As expected, the laminar and quasi-turbulent flow regimes in Fig. 7 showed no significant difference between the contraction ratios. Similar to the friction factor results (Fig. 6), a decrease in the contraction ratio caused a delay in the entire transitional flow regime for the square-edged inlet (Fig. 7(a)), while transition occurred earlier for the re-entrant inlet (Fig. 7(b)). It can therefore also be concluded that for a fixed flow-calming section, an increase in test section diameter will not only affect the transitional

flow regime due to the changes the buoyancy effects [7, 11], but also due to the changes the inlet contraction ratio.
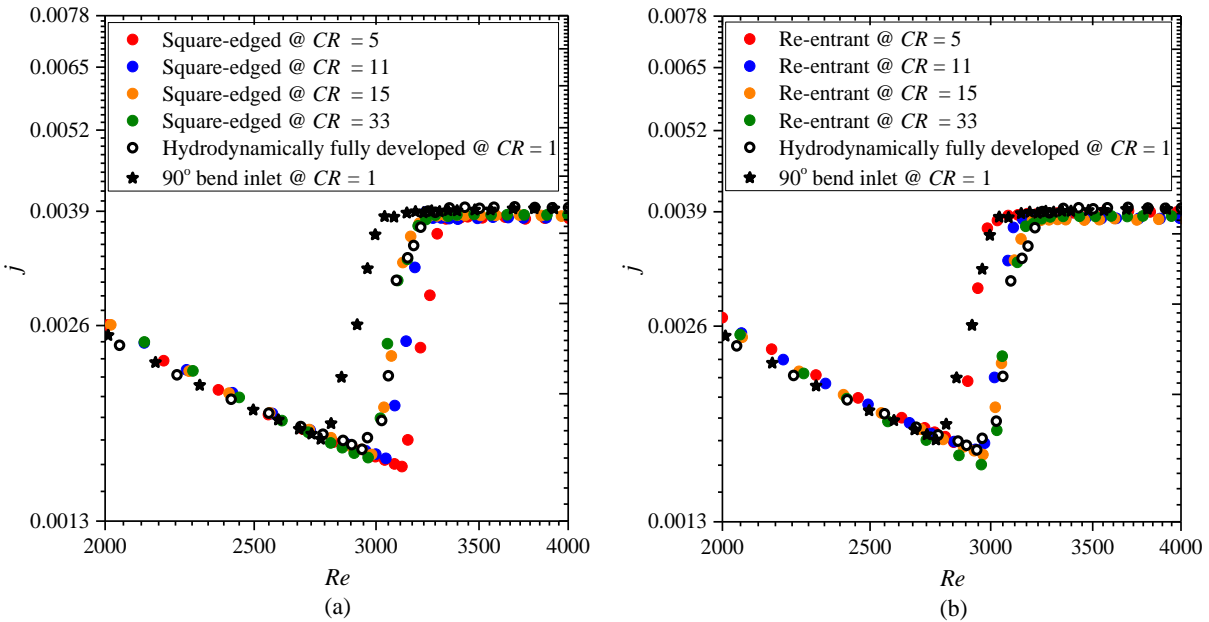


**Fig. 7: Comparison of the fully developed Colburn $j$-factors as a function of Reynolds number for different contraction ratios using (a) square-edged inlet and (b) re-entrant inlet at a heat flux of 8 kW/m$^2$.**

To investigate the effect of inlet disturbances on the boundaries of the transitional flow regime, Fig. 8 compares the Reynolds numbers at which transition started (red) and ended (blue) for the different types of inlets as a function of contraction ratio at a heat flux of 8 kW/m$^2$. For the square-edged inlet, both the Reynolds numbers at which transition started ($Re_{cr}$) and ended ($Re_{qt}$) decreased with increasing inlet contraction ratios. Therefore, a lower contraction ratios led to a smoother inlet that caused transition to be delayed [9]. However, for the re-entrant inlet, the Reynolds numbers at which transition started and ended increased with increasing contraction ratio but remained lower than for the square-edged inlet. As the contraction ratio decreased, the disturbances increased, which caused transition to occur earlier (at lower Reynolds numbers). At the maximum contraction ratio of 33, the transition Reynolds numbers for both inlets were approximately the same and also corresponded to the hydrodynamically fully developed (FD) inlet. This implies that the boundaries of the transitional flow regime were affected by the different inlet geometries when the contraction ratios were relatively low, but not when the contraction ratio is higher than 33. The 90° bend inlet had the lowest Reynolds numbers for both the start and end of

the transitional flow regime. This was as expected because a greater inlet disturbance was created at the inlet of the test section due to the 90° bend. Furthermore, Fig. 8 also indicated that the width of the transitional flow regime ($\Delta Re = Re_{qt} - Re_{cr}$, as defined by Everts and Meyer [11]) for the square-edged and re-entrant inlet geometries, increased with increasing contraction ratio.
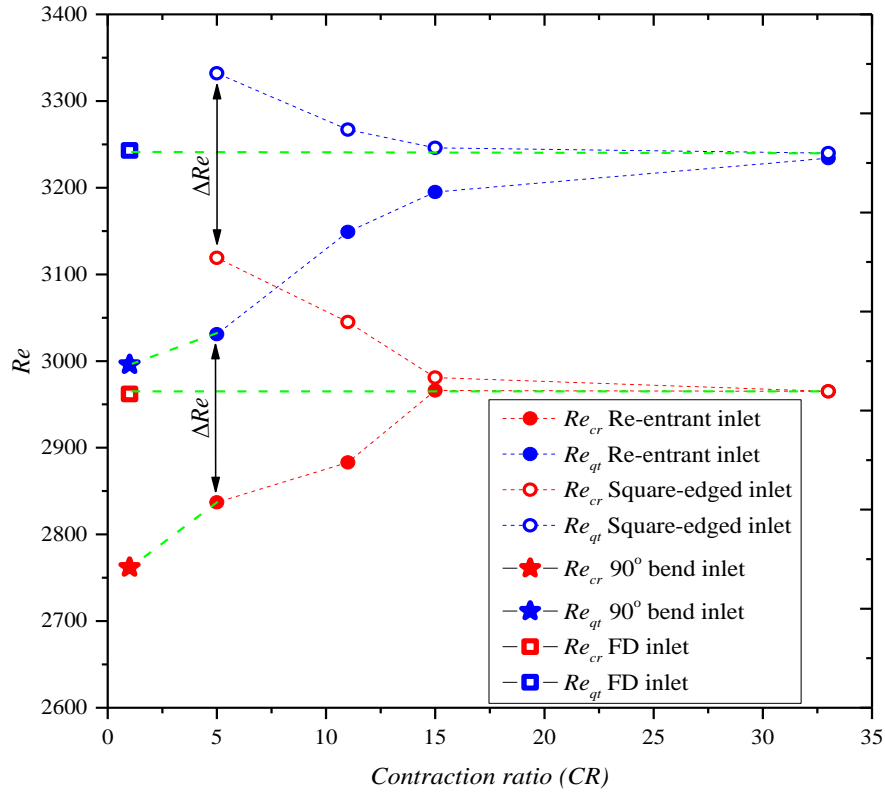


**Fig. 8: Comparison of the Reynolds numbers at which transition started ($Re_{cr}$) and ended ($Re_{qt}$) as a function of contraction ratio for the different inlet geometries at a heat flux of 8 kW/m². "FD" in the legend indicates hydrodynamic fully developed inlet.**

The Reynolds numbers at which transition started (Fig. 9(a)) and ended (Fig. 9(b)) are compared for the square-edged and re-entrant inlets as a function of heat flux. As expected [2], both the Reynolds numbers at which transition started and ended increased with increasing heat flux. However, the rate of this increase differed for the different inlets and contraction ratios. Fig. 9(c) and (d) compare the difference between the transition Reynolds numbers of the square-edged and re-entrance inlets, $\Delta Re_{inlets} = Re_{squ} - Re_{ree}$, at the start and end of the transitional flow regime, as a function of heat flux.
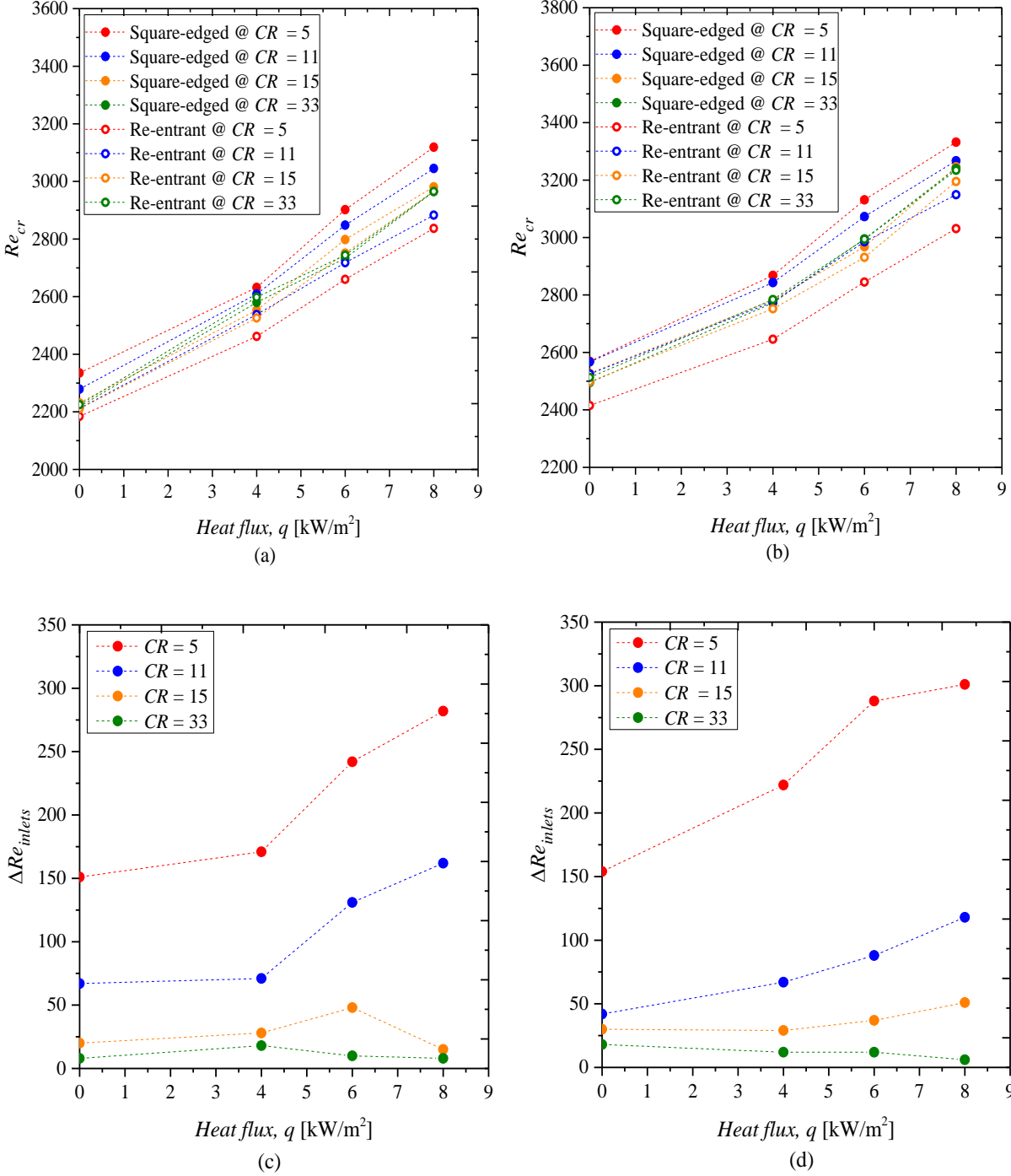
29

**Fig. 9: Comparison of the Reynolds number at which transition (a) started and (b) ended of transition, as well as the difference between the square-edged and re-entrant inlets at the (c) start ($\Delta Re_{inlets} = Re_{squ} - Re_{ree}$) and (d) end ($\Delta Re_{inlets} = Re_{squ} - Re_{ree}$) of the transitional flow regime, as a function of heat flux.**

At lower contraction ratios (≤11), the rate of increase of Reynolds numbers with heat flux for the square-edged inlet was slightly more than for the re-entrant inlet. However, at higher

contraction ratios (>11), the difference between the transition Reynolds numbers of the square-edged and re-entrant inlets became negligible. According to Nagendra [27], for all flow regimes, the influence of inlet disturbances decreased with increasing values of $ReRa(D/L)$ and become insignificant for $ReRa(D/L) > 10^6$. At the maximum heat flux of 8 kW/m$^2$ and a contraction ratio of 5, the value of $ReRa(D/L)$ was $1.42 \times 10^5$. This is why for heat fluxes lower than 8 kW/m$^2$, the effect of inlet disturbances on the transitional flow regime were significant for all the inlets.

Mori et al. [28] found that for high levels of inlet disturbances, the critical Reynolds numbers increased with increase in Rayleigh numbers, because buoyancy effects supressed the disturbances generated at the inlet. This explains why for lower contraction ratios such as 5 and 11, the difference between the Reynolds numbers of the square-edged and re-entrant inlets increased with increasing heat flux ($Gr$ or $Gr^*$) in Fig. 9(c) and (d). The green markers in Fig. 9 indicate that at the maximum contraction ratio (33), the Reynolds number difference ($\Delta Re_{inlets}$) at both the start (Fig. 9(c)) and end (Fig. 9(d)) of transition remained approximately zero for all the heat fluxes.

### 3.2.3   Summary

Fig. 10 gives an easier schematic representation of the influence of contraction ratio on the fully developed heat transfer coefficients for a square-edged inlet (blue lines) and a re-entrant inlet (green lines). As was found by previous studies [2, 9, 13, 17, 22] different inlet conditions did not affect the heat transfer coefficients in the laminar, quasi-turbulent and turbulent flow regimes; however, the transitional flow regime was significantly affected. When a re-entrant inlet was used, the light green to dark green lines indicate that transition is delayed when the contraction ratio was increased up to the maximum contraction ratio of 33, which is represented by the red line. The opposite exists when a square-edged inlet was used. As indicated by the light blue to dark blue lines, an increase in contraction ratio led to an earlier transition. The "converged" solid red line not only represented the results of the square-edged and re-entrant inlet geometries when a higher contraction ratio was used, but also the hydrodynamically fully developed inlet.
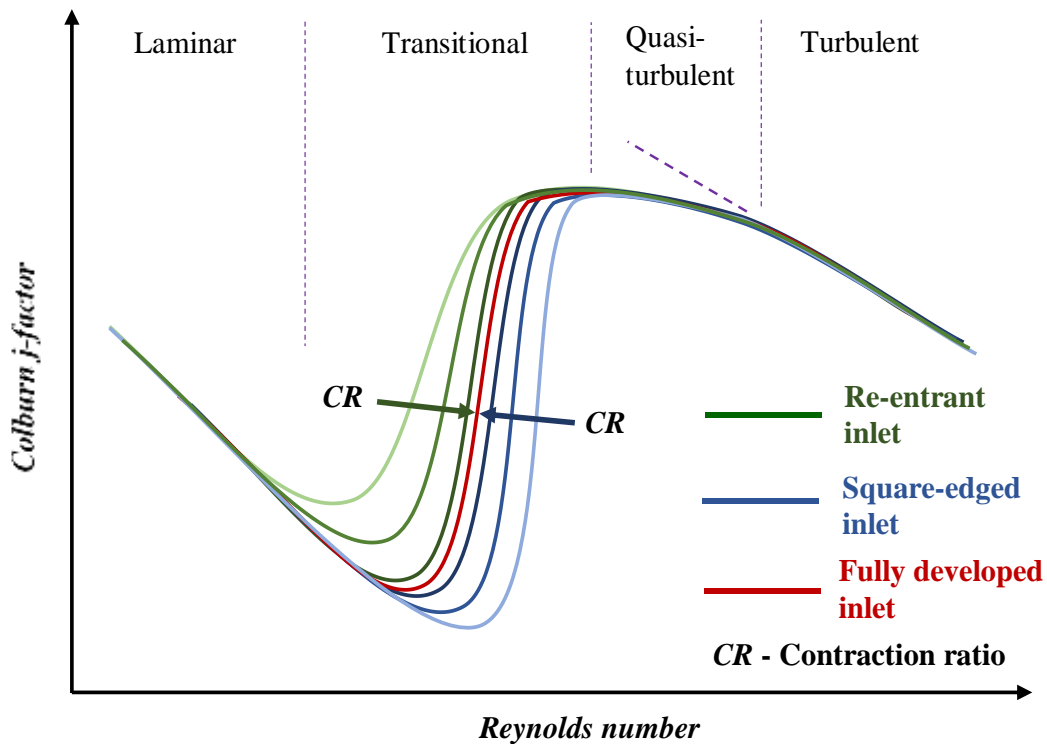
**Fig. 10: Schematic representation of the influence of contraction ratio on the fully developed Colburn *j*-factor as a function of Reynolds number for a square-edged (blue) and a re-entrant (green) inlet.**

Fig. 11 and Fig. 12 show qualitatively (without CFD simulations) the schematic representation of the fluid flow pattern for square-edged and re-entrant inlets respectively, with different contraction ratios. For the square-edged inlet (Fig. 11), as the contraction ratio decreased, the inlet cross-sectional area where the eddies formed, decreased. The fluid flow pattern to the test section therefore became smoother (with less disturbances) and transition was delayed (higher Reynolds numbers) [9]. For the re-entrant inlet (Fig. 12), the protrusion of the tube caused more disturbances compared with the square-edged inlet. Furthermore, as the cross-sectional area decreased (by decreasing the contraction ratio), the inlet disturbances increased as well, which caused transition to occur at lower Reynolds numbers. At higher contraction ratios (>33), the inlet geometry had a negligible influence on the transitional flow regime and the results were similar to that of a hydrodynamically fully developed inlet.
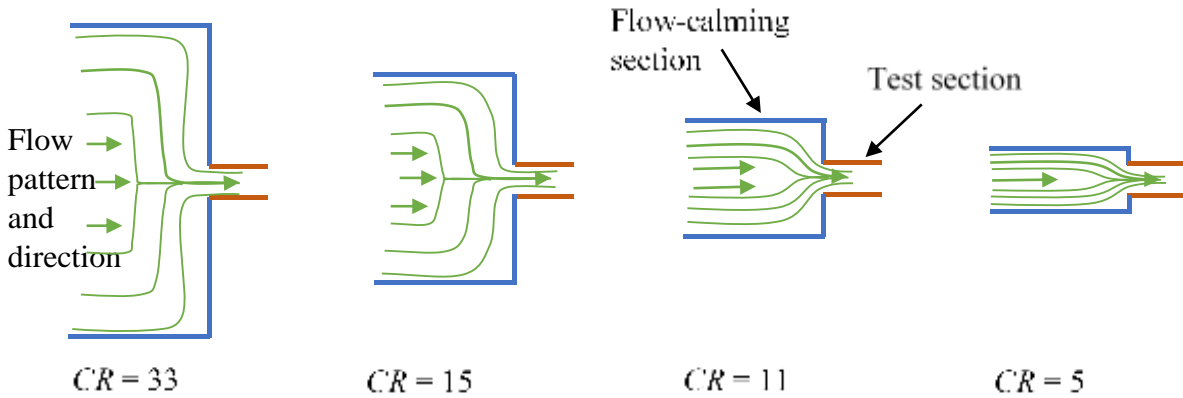
**Fig. 11: Schematic diagram of the fluid flow pattern for a square-edged inlet with different contraction ratios.**
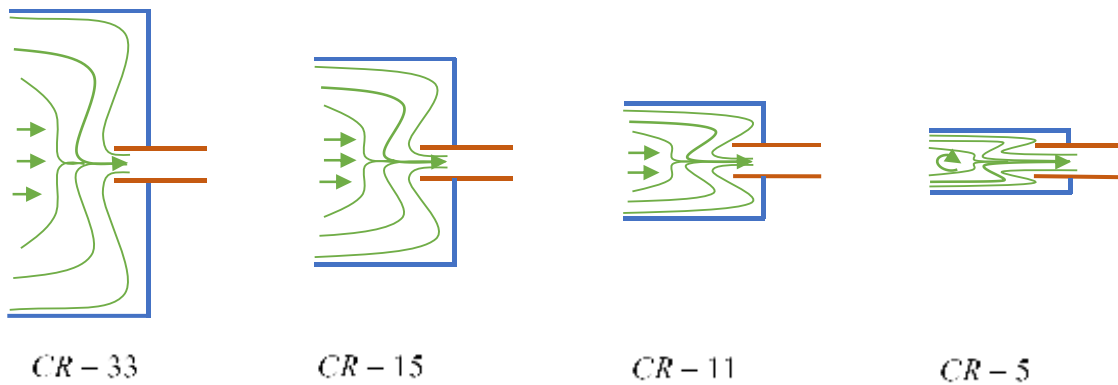


**Fig. 12: Schematic diagram of the fluid flow pattern for a re-entrant inlet with different contraction ratios.**

## 3.3 Recommendations for future work

It was not the purpose of this study to investigate the flow distributions and characteristics at the inlet with CFD. It is therefore recommended that a CFD study be conducted to investigate in more detail the qualitatively descriptions of the flow for the different types of inlets and specifically the flow patterns in Fig. 11 and Fig. 12.

As this experimental study indicated that the boundaries of the transitional flow regime, as well as the heat transfer and pressure drop characteristics in the transitional flow regime were affected by contraction ratios, it is important that future work should also quantify contraction ratios when developing correlations for specific inlets. Furthermore, the contraction ratio or size of a heat exchanger header/plenum should be taken into account in the design of heat exchangers operating in the transitional flow regime. What also needs to be investigated is the length (or

33

aspect ratios) of calming sections to determine what effect it will have on the transitional flow regime.

## 4. Conclusions

This paper investigated the effect of inlet disturbances on the heat transfer and pressure drop characteristics in the transitional flow regime using a square-edged and re-entrant inlet with different contraction ratios. Furthermore, a hydrodynamically fully developed and 90º bend inlets were also investigated. An experimental set-up that was able to accommodate the flow-calming sections with different inlet geometries and contraction ratios was used. Four flow-calming sections with different diameters corresponding to a contraction ratio of 5, 11, 15 and 33 were investigated. Experiments were conducted between Reynolds numbers of 1 000 and 6 000, using water. Furthermore, the test section was heated at constant heat fluxes of 4, 6 and 8 kW/m$^2$.

It was found that for the square-edged and re-entrant inlets, the flow-calming section contents had no influence on the heat transfer and pressure drop characteristics in the laminar, transitional and quasi-turbulent flow regimes. As the contraction ratio increased, transition occurred earlier for the square-edged inlet, while for the re-entrant inlet, transition was delayed with increasing contraction ratios. For contraction ratios larger than 33, transition occurred at approximately the same critical Reynolds numbers for both the square-edged and re-entrant inlets, which also corresponded to the critical Reynolds numbers of the hydrodynamically fully developed inlet. For the 90º bend inlet, transition occurred earlier than all the other inlet geometries and contraction ratios. The effect of heating on the transition Reynolds numbers was more at lower contraction ratios than at higher contraction ratios for both the square-edged and re-entrant inlets.

# References

[1] J.P. Meyer, Heat transfer in tubes in the transitional flow regime, in: Proceedings of the 15th International Heat Transfer Conference, IHTC-15, Kyoto, Japan, 2014, pp. 1-21.

[2] A.J. Ghajar, L.M. Tam, Heat transfer measurements and correlations in the transition region for a circular tube with three different inlet configurations, Experimental Thermal and Fluid Science, 8(1) (1994) 79-90.

[3] A.J. Ghajar, L.M. Tam, Laminar-transition-turbulent forced and mixed convective heat transfer correlations for pipe flows with different inlet configurations, American Society of Mechanical Engineers, Heat Transfer Division, (Publication) HTD, (1991) 15-23.

[4] L.M. Tam, A.J. Ghajar, Transitional heat transfer in plain horizontal tubes, Heat Transfer Engineering, 27(5) (2006) 23-38.

[5] A.J. Ghajar, L.M. Tam, Flow regime map for a horizontal pipe with uniform wall heat flux and three inlet configurations, Experimental Thermal and Fluid Science, 10(3) (1995) 287-297.

[6] A.J. Ghajar, L.M. Tam, S.C. Tam, Improved heat transfer correlation in the transition region for a circular tube with three inlet configurations using artificial neural networks, Heat Transfer Engineering, 25(2) (2004) 30-40.

[7] J.P. Meyer, M. Everts, Single-phase mixed convection of developing and fully developed flow in smooth horizontal circular tubes in the laminar and transitional flow regimes, International Journal of Heat and Mass Transfer, 117 (2018) 1251-1273.

[8] M. Everts, J.P. Meyer, Relationship between pressure drop and heat transfer of developing and fully developed flow in smooth horizontal circular tubes in the laminar, transitional, quasi-turbulent and turbulent flow regimes, International Journal of Heat and Mass Transfer, 117 (2018) 1231-1250.

[9] J.P. Meyer, S.M. Abolarin, Heat transfer and pressure drop in the transitional flow regime for a smooth circular tube with twisted tape inserts and a square-edged inlet, International Journal of Heat and Mass Transfer, 117 (2018) 11-29.

[10] J. Dirker, J.P. Meyer, D.V. Garach, Inlet flow effects in micro-channels in the laminar and transitional regimes on single-phase heat transfer coefficients and friction factors, International Journal of Heat and Mass Transfer, 77 (2014) 612-626.

[11] J.P. Meyer, M. Everts, A.T.C. Hall, F.A. Mulock-Houwer, M. Joubert, L.M.J. Pallent, E.S. Vause, Inlet tube spacing and protrusion inlet effects on multiple circular tubes in the laminar, transitional and turbulent flow regimes, International Journal of Heat and Mass Transfer, 118 (2018) 257-274.

[12] J.P. Meyer, T.J. McKrell, K. Grote, The influence of multi-walled carbon nanotubes on single-phase heat transfer and pressure drop characteristics in the transitional flow regime of smooth tubes, International Journal of Heat and Mass Transfer, 58(1-2) (2013) 597-609.

[13] A.J. Ghajar, K.F. Madon, Pressure drop measurements in the transition region for a circular tube with three different inlet configurations, Experimental Thermal and Fluid Science, 5(1) (1992) 129-135.

[14] A.I. Bashir, M. Everts, J.P. Meyer, R. Bennacer, Single-phase forced convection heat transfer and pressure drop in circular tubes in the laminar and transitional flow regimes, Experimental Thermal and Fluids Science, Manuscript nr: ETFS_2019_411, Submitted on 22 March 2019 (2019).

[15] L.M. Tam, A.J. Ghajar, The unusual behavior of local heat transfer coefficient in a circular tube with a bell-mouth inlet, Experimental Thermal and Fluid Science, 16(3) (1998) 187-194.

[16] A.J. Ghajar, C.C. Tang, W.L. Cook, Experimental investigation of friction factor in the transition region for water flow in minitubes and microtubes, Heat Transfer Engineering, 31(8) (2010) 646-657.

[17] L.M. Tam, A.J. Ghajar, Effect of inlet geometry and heating on the fully developed friction factor in the transition region of a horizontal tube, Experimental Thermal and Fluids Science, 1777(97) (1997) 52-64.

[18] K.H. Tam, L.M. Tam, A.J. Ghajar, Effect of inlet geometries and heating on the entrance and fully-developed friction factors in the laminar and transition regions of a horizontal tube, Experimental Thermal and Fluid Science, 44 (2013) 680-696.

[19] L.M. Tam, A.J. Ghajar, H.K. Tam, Contribution analysis of dimensionless variables for laminar and turbulent flow convection heat transfer in a horizontal tube using artificial neural network, Heat Transfer Engineering, 29(9) (2008) 793-804.

[20] Y.A. Çengel, A.J. Ghajar, Heat and Mass Transfer: Fundamentals & Applications, 5th ed., Mcgraw Hill, New York, 2015.

[21] J.P. Meyer, J.A. Olivier, Transitional flow inside enhanced tubes for fully developed and developing flow with different types of inlet disturbances: Part II – heat transfer, International Journal of Heat and Mass Transfer, 54(7-8) (2011) 1598-1607.

[22] J.A. Olivier, J.P. Meyer, Single-phase heat transfer and pressure drop of the cooling of water inside smooth tubes for transitional flow with different inlet geometries (RP-1280), HVAC&R Research, 16(4) (2010) 471-496.

[23] J.P. Meyer, A.I. Bashir, M. Everts, Single-phase mixed convective heat transfer and pressure drop in the laminar and transitional flow regimes in smooth inclined tubes heated at a constant heat flux, Experimental Thermal and Fluids Science, Manuscript nr: ETFS_2019_410, Submitted on 22 March 2019 (2019).

[24] S.M. Abolarin, M. Everts, J.P. Meyer, Heat transfer and pressure drop characteristics of alternating clockwise and counter clockwise twisted tape inserts in the transitional flow regime, International Journal of Heat and Mass Transfer, 133 (2019) 203-217.

[25] S.M. Abolarin, M. Everts, J.P. Meyer, The influence of peripheral u-cut twisted tapes and ring inserts on the heat transfer and pressure drop characteristics in the transitional flow regime, International Journal of Heat and Mass Transfer, 132 (2019) 970-984.

[26] D.D. Ndenguma, J. Dirker, J.P. Meyer, Transitional flow regime heat transfer and pressure drop in an annulus with non-uniform wall temperatures, International Journal of Heat and Mass Transfer, 108 (2017) 2239-2252.

[27] H.R. Nagendra, Interaction of free and forced convection in horizontal tubes in the transition regime, Journal of Fluid Mechanics, 57(2) (1973) 269-288.

[28] M. Yasuo, F. Kozo, T. Shinobu, N. Masakuni, Forced convective heat transfer in uniformly heated horizontal tubes 1st report—Experimental study on the effect of buoyancy, International Journal of Heat and Mass Transfer, 9(5) (1966) 453-463.

[29] M. Al-Arabi, Turbulent heat transfer in the entrance region of a tube, Heat Transfer Engineering, 3(3-4) (1982) 76-83.

[30] H.A. Mohammed, The effect of different inlet geometries on laminar flow combined convection heat transfer inside a horizontal circular pipe, Applied Thermal Engineering, 29(2) (2009) 581-590.

[31] M. Everts, Single-phase mixed convection of developing and fully developed flow in smooth horizontal circular tubes in the laminar, transitional, quasi-turbulent and turbulent flow regimes, PhD thesis, University of Pretoria, Pretoria, 2018.

[32] M. Everts, Heat transfer and pressure drop of developing flow in smooth tubes in the transitional flow regime, Masters dissertation, University of Pretoria, Pretoria, 2014.

[33] A. Bakker, R.D. LaRoche, E.M. Marshall, Laminar flow in static mixers with helical elements, in: The Online CFM Book (2000).

[34] R.E. Rayle, Influence of orifice geometry on static pressure measurements, ASME paper No 59-A-234, (1959).

[35] C.O. Popiel, J. Wojtkowiak, Simple formulas for thermophysical properties of liquid water for heat transfer calculations (from 0°C to 150°C), Heat Transfer Engineering, 19(3) (1998) 87-101.

[36] M. Everts, J.P. Meyer, Heat transfer of developing and fully developed flow in smooth horizontal tubes in the transitional flow regime, International Journal of Heat and Mass Transfer, 117 (2018) 1331-1351.

[37] P.F. Dunn, Measurement and Data Analysis for Engineering and Science, CRC press, United States of America, 2010.

[38] J.L. Poiseuille, Recherches expérimentales sur le mouvement des liquides dans les tubes de très- petits diamètres, Imprimerie Royale, (1844).

[39] H. Blasius, Das ähnlichkeitsgesetz bei reibungsvorgangen in flüssigkeiten, Forschg. Arb. Ing.-Wes, (1913) 131-137.

[40] S.M. Morcos, A.E. Bergles, Experimental investigation of combined forced and free laminar convection in horizontal tubes, Journal of Heat Transfer, 97(2) (1975) 212-219.

[41] V. Gnielinski, New equations for heat and mass-transfer in turbulent pipe and channel flow, International Chemical Engineering, 16(2) (1976) 359-368.

[42] J.P. Meyer, M. Everts, N. Coetzee, K. Grote, M. Steyn, Heat transfer coefficients of laminar, transitional, quasi-turbulent and turbulent flow in circular tubes, International Communications in Heat and Mass Transfer, 105 (2019) 84-106.